Liquid Crystals
Publication details, including instructions for authors and subscription information:
http://www.informaworld.com/smpp/title~content=t713926090

Simulation of reorientation dynamics in bipolar nematic droplets

Philip K. Chan; Alejandro D. Rey

Online publication date: 29 June 2010

To cite this Article Chan, Philip K. and Rey, Alejandro D.(1997) 'Simulation of reorientation dynamics in bipolar nematic droplets', Liquid Crystals, 23: 5, 677 — 688
To link to this Article: DOI: 10.1080/026782997207957
URL: http://dx.doi.org/10.1080/026782997207957

LIQUID CRYSTALS, 1997, VOL. 23, NO. 5, 677–688

Simulation of reorientation dynamics in bipolar nematic droplets

by PHILIP K. CHAN* and ALEJANDRO D. REY
Department of Chemical Engineering, McGill University, 3480 University, Montreal, Quebec, H3A 2A7, Canada

(*Received 5 May 1997; accepted 20 June 1997*)

A two-dimensional model composed of a synthesis of the Leslie–Ericksen continuum theory of nematics and the Euler–Lagrange equation for surface director motion is used to study the magnetic-induced director reorientation dynamics confined in spherical bipolar droplets with viscoelastic surfaces. The magnetic field is restricted to the droplet axis of symmetry direction. The numerical results indicate that the surface viscosity and anchoring strength must be taken into account to describe accurately director reorientation dynamics in droplets. In addition, the numerical results replicate frequently reported experimental observations on the performance of polymer dispersed liquid crystal films. These observations include the familiar exponential increase followed by saturation in light transmittance as the external applied field increases, and the exponential increase (decrease) followed by saturation as time increases in the on (off) state. Furthermore, this model is able to predict precisely the relationships between the rise and decay times and the external applied field strength, and the fact that the switching field strength is inversely proportional to droplet size.

1. Introduction

Nematic liquid crystals in confined geometries are a subject of current interest because of the practical and potential display applications of polymer dispersed liquid crystal (PDLC) films [1–6]. Typical applications are switchable windows and billboards. These films are composed of micron-size liquid crystalline droplets dispersed uniformly in a solid polymer matrix. The director configuration within the droplets controls the electro-optical properties of PDLCs. The film becomes transparent when an electric or magnetic field is applied normally to it, since the directors tend to align with the field direction and the ordinary index of refraction of the nematic liquid crystal is by design equal to the polymer matrix index of refraction. The optical response to an electric field is similar to that due to a magnetic field [3]. On removing the field, the directors reorient to their equilibrium configuration and the film becomes opaque. While various factors affect the performance of PDLC devices, two are due to the liquid crystalline droplets. Firstly, the rate of director reorientation within the droplet affects the rise and decay times when the external field is turned on and off, respectively. Secondly, the director configuration in the on and off states affects the film contrast. These factors are attributed to the relative magnitude of the Frank elastic constant, surface anchoring strength, external field strength, and bulk and surface viscosities.

*Author for correspondence.

In the absence of an external field, the director configuration within a droplet is determined by a balance between the bulk and surface forces, which are represented by the Frank elastic constants (K_{11}, K_{22} and K_{33}) and surface anchoring strength (W_o), respectively [7]. For strong surface anchoring strength, the surface directors remain undeterred by the bulk torques and defects are usually formed in a spherical cavity. Examples are the radial configuration with one point defect in the droplet centre for perpendicular anchoring, and the bipolar configuration with two point defects located at the ends of the axis of symmetry for tangential anchoring. The bipolar configuration is predominately used in PDLC applications, and is the focus of this paper. For weak surface anchoring, the surface and bulk forces compete, and this results in a configuration with less curvature. If the anchoring strength is low enough, surface defects, such as the ones present in bipolar droplets, can disappear [6]. In the presence of an external electric or magnetic field, the transient director configuration is a balance between the bulk, surface, and external torques.

The bipolar configuration was theoretically determined by Dubois-Violette and Parodi [8], and experimentally verified by Candau *et al.* [9]. Recently, studies on the bipolar configuration have intensified, because of its usage in PDLCs. Most polymers tend to induce the surface director to align tangentially to the cavity wall [6]. Vilfan *et al.* [10], and Huang and Tuthill [11] numerically studied the steady-state director configuration close to the nematic–isotropic transition point.

Ding *et al.* [12], experimentally looked at the steady-state optical patterns of bipolar droplets that have undergone reorientation due to an electric field. These studies have improved the current understanding of bipolar droplets at the steady state. They do not, however, study the transient director reorientation phenomena when an external field is applied and then removed, as is typical in PDLC devices. Drzaic [13], and Jain and Rout [14] experimentally studied the reorientation dynamics in bipolar droplets, and offered a multi-stage model to explain their data. In addition, Wu *et al.* [15], proposed a simple model to explain their experimental results on the response times and voltages for PDLC light shutters. A fundamental understanding of the transient reorientation dynamics in nematic droplets is an essential ingredient to improve the design and control of PDLC devices. This paper intends to provide such an understanding by studying numerically the director reorientation dynamics in bipolar droplets. Previous steady-state numerical studies exist for director configurations with perpendicular surface alignment and weak anchoring [16, 17].

The static interaction between a nematic liquid crystal and a bounding surface is described macroscopically by a surface free energy. This free energy is composed of both the surface deformation energy and the coupling energy of the director at the surface [18]. The surface deformation energy is due to director gradients at the surface and is introduced by surface elastic constants. This energy can be neglected since it does not significantly influence the director configuration inside a droplet [6]. The coupling energy depends on the orientation of the surface director with respect to the easy axis of the surface, which is the preferred surface director orientation. The easy axis depends on the specific interaction between the liquid crystal and bounding surface, and on any surface treatment. The coupling energy, introduced into the surface free energy by the anchoring strength W_o [7], is a minimum when the director is aligned along the easy axis. When $W_o \to \infty$, the director aligns along the easy axis (strong anchoring), and when W_o is finite, the time dependent surface director is obtained from the balance between surface elastic and viscous torques about an axis normal to the surface. The surface elastic torques are due to bulk director deformations impressed onto the surface, surface director gradients, and deviations of the surface director from the easy axis. Viscous torques are created from the transient director reorientation and are introduced by surface viscosities. This theory has been successful in describing the periodic twist instability of nematic polymers due to a magnetic field [19].

The objective of this paper is to present results from a two-dimensional numerical study on the transient director configuration in a bipolar spherical droplet for the following two cases: (*a*) director relaxation from a distorted configuration, and (*b*) director reorientation due to a magnetic field applied along the droplet axis of symmetry. The model incorporates the Leslie–Ericksen continuum theory [7] for bulk director reorientation, the Euler–Lagrange equation [20] for surface director motion, and a free energy density composed of the Frank theory [7] for bulk distortion and the Rapini–Papoular theory [21] for surface distortion. The rest of this paper is organized as follows. The governing equations, auxiliary conditions, and the method of solution are given in § 2. The numerical results are presented, discussed, and contrasted with experimental data in § 3. Finally, conclusions are given in § 4.

2. Problem formulation and numerical methods

This section is divided into two parts. Theory is given in the first part, while the second part presents the derivation of the governing equations and numerical methods employed to solve them.

2.1. *Theory*

According to the Leslie–Ericksen theory [7], director reorientation is governed by the following torque balance equation written in Cartesian tensorial notation:

$$\Gamma_e + \Gamma_v + \Gamma_m = 0 \tag{1}$$

where the three terms on the left-hand side, respectively, denote the elastic, viscous and magnetic torques on the director per unit volume. Their constitutive equations are as follows:

$$\Gamma_e = -\mathbf{n} \times \frac{\delta f_d}{\delta \mathbf{n}} \tag{2a}$$

$$\Gamma_v = -\mathbf{n} \times (\gamma_1 \mathbf{N} + \gamma_2 \mathbf{A}\ \mathbf{n}) \tag{2b}$$

$$\Gamma_m = \chi_a (\mathbf{n}\ \mathbf{H})\mathbf{n} \times \mathbf{H} \tag{2c}$$

with viscosities:

$$\gamma_1 = \alpha_3 - \alpha_2 \tag{3a}$$

$$\gamma_2 = \alpha_2 + \alpha_3. \tag{3b}$$

The viscosities α_2 and α_3 are two of the six Leslie viscosities. The term $\delta f_d/\delta \mathbf{n}$ denotes the functional derivative of the distortion free energy density f_d with respect to the director $\mathbf{n}$, χ_a is the magnetic susceptibility anisotropy, and $\mathbf{H}$ is the magnetic field. The kinematic quantities appearing in the constitutive equations are defined as follows:

$$\mathbf{N} = \dot{\mathbf{n}} - \Omega\ \mathbf{n} \tag{4a}$$

$$\Omega = [(\nabla \mathbf{v})^T - \nabla \mathbf{v}]/2 \tag{4b}$$

$$\mathrm{A} = [(\nabla \mathbf{v})^T + \nabla \mathbf{v}]/2 \tag{4c}$$

where $\mathbf{v}$ is the velocity field, $\mathbf{N}$ is the angular velocity of the director relative to that of the fluid, Ω is the vorticity tensor and A is the rate of deformation tensor. The superposed dot denotes the material time derivative.

The total free energy is expressed as follows [7]:

$$F = \int_V f_d \, dV + \int_V f_m \, dV + \int_S f_s \, dS \tag{5}$$

where f_d, f_m and f_s are the distortion, magnetic and surface free energy densities, respectively, and are defined as follows [7, 21]:

$$f_d = \frac{1}{2}K_{11}(\nabla \mathbf{n})^2 + \frac{1}{2}K_{22}(\mathbf{n} \nabla \times \mathbf{n})^2 + \frac{1}{2}K_{33}\|\mathbf{n} \times \nabla \times \mathbf{n}\|^2 \tag{6a}$$

$$f_m = -\frac{1}{2}\chi_a(\mathbf{n} \mathbf{H})^2 \tag{6b}$$

$$f_s = \frac{1}{2}W_o \sin^2(\phi - \phi_o) \tag{6c}$$

where K_{11}, K_{22} and K_{33} are the splay, twist and bend elastic constants, respectively, W_o is the surface anchoring strength, and ϕ and ϕ_o are the actual and preferred anchoring angles at the droplet surface, respectively.

The Euler–Lagrange equation for surface motion previously derived [19] is used here to formulate the balance of surface elastic and viscous torques. Assuming no positional slip, the Euler–Lagrange equation is written as follows [19]:

$$\frac{\partial R^s}{\partial \dot{\phi}} + \Phi_\phi = 0 \tag{7}$$

where R^s is the surface Rayleigh dissipation function, Φ_ϕ represents the elastic forces, and a superposed dot denotes time differentiation. Since the frictional force $\partial R^s/\partial \dot{\phi}$ is a linear function of the velocities, R^s is given as

$$R^s = \lambda^s(\dot{\phi})^2 \tag{8}$$

where λ^s is the surface viscosity for the surface director reorientation. Surface viscosity governing surface director reorientation dynamics have been confirmed experimentally by Oliveira *et al.* [22].

The elastic forces are acquired from the surface contribution to the variation of the total free energy of the system. This energy is composed of both bulk (i.e. elastic and magnetic) and surface contributions. In a planar orientation mode [i.e. $\mathbf{n} = \mathbf{n}(\phi)$], the total free energy, according to equations (5) and (6), can be expressed as follows:

$$F = \int_V f_d(\phi, \nabla\phi) \, dV + \int_V f_m(\phi) \, dV + \int_S f_s(\phi) \, dS. \tag{9}$$

The variation of F is

$$\delta F = \int_V \left(\frac{\partial f_d}{\partial \phi}\delta\phi + \frac{\partial f_m}{\partial \phi}\delta\phi + \frac{\partial f_d}{\partial \nabla\phi}\delta\nabla\phi \right) dV + \int_S \frac{\partial f_s}{\partial \phi}\delta\phi \, dS. \tag{10}$$

Using the divergence theorem, δF becomes

$$\delta F = \int_V \left(\frac{\partial f_d}{\partial \phi}\delta\phi + \frac{\partial f_m}{\partial \phi}\delta\phi - \nabla \frac{\partial f_d}{\partial \nabla\phi}\delta\nabla\phi \right) dV + \int_S \left(\frac{\partial f_d}{\partial \nabla\phi}\delta\phi \, \nu + \frac{\partial f_s}{\partial \phi}\delta\phi \right) dS \tag{11}$$

where ν is the outward unit normal vector to the enclosing surface S of volume V. Therefore, the elastic forces at the surfaces are expressed as follows:

$$\Phi_\phi = \frac{\partial f_d}{\partial \nabla\phi} \, \nu + \frac{\partial f_s}{\partial \phi}. \tag{12}$$

2.2. *Governing equations and auxiliary conditions*

Figure 1 shows a cross section of a bipolar droplet and defines the cylindrical coordinate system (r, θ, z). ϕ is the polar angle measured from the z axis and is the only angle considered in this paper. Since bipolar droplets have axisymmetry, this paper is restricted to a two-dimensional study of the magnetic-induced director reorientation dynamics inside a circle of radius R. In addition, the magnetic field is parallel to the z axis; i.e.

$$\mathbf{H} = (0, 0, H). \tag{13}$$

It is assumed that the characteristic times of the velocity variations are much faster than those of the director; i.e. the velocity follows the director instantaneously [23]. Consequently, backflow effects are neglected. The transient planar two-dimensional director field is defined as follows:

$$\mathbf{n}(r, z, t) = (\sin\phi(r, z, t), 0, \cos\phi(r, z, t)) \tag{14}$$

where the unit length constraint, $\mathbf{n}\,\mathbf{n} = 1$, is automatically satisfied.

The equation that governs the behaviour of ϕ is the θ component of the torque balance [equation (1)]. The following scalings are used to nondimensionalize the governing equation:

$$K_{ii}^* = \frac{K_{ii}}{K} \quad (\text{for } i = 1, 2, 3), \qquad K = \frac{1}{2}(K_{11} + K_{33}),$$

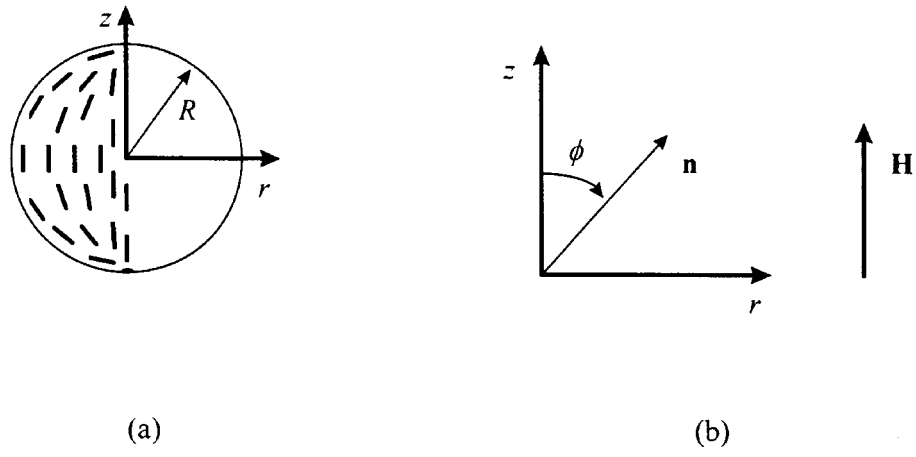

Figure 1. Schematic representation of the cross section of a bipolar droplet and definition of the cylindrical coordinate system. The z axis is along the axis of symmetry, which is the line joining the two point defects. R is the circle radius, ϕ is the polar angle, $\mathbf{n}$ is the director and $\mathbf{H}$ is the magnetic field.

$$r^* = \frac{r}{R}, \qquad z^* = \frac{z}{R}, \qquad t^* = \frac{tK}{\gamma_1 R^2},$$

and

$$Z_o = \frac{\chi_a H^2 R^2}{K}.$$

The dimensionless Zocher number Z_o gives the relative magnitude of magnetic to elastic torques. The superscripted asterisks denote dimensionless variables. By incorporating equations (1)–(6), (13) and (14), and using the scaling relations given above, the following dimensionless time-dependent second-order nonlinear partial differential equation is obtained to describe the magnetic-induced director reorientation dynamics:

$$\frac{\partial \phi}{\partial t^*} = \kappa_1 + \kappa_2 \frac{\partial \phi}{\partial r^*} + \kappa_3 \frac{\partial \phi}{\partial r^*}\frac{\partial \phi}{\partial r^*} + \kappa_4 \frac{\partial^2 \phi}{\partial r^{*2}} + \kappa_5 \frac{\partial \phi}{\partial z^*} + \kappa_6 \frac{\partial \phi}{\partial z^*}\frac{\partial \phi}{\partial z^*} + \kappa_7 \frac{\partial^2 \phi}{\partial z^{*2}} + \kappa_8 \frac{\partial \phi}{\partial r^*}\frac{\partial \phi}{\partial z^*} + \kappa_9 \frac{\partial^2 \phi}{\partial r^* \partial z^*} - \frac{1}{2} Z_o \sin(2\phi) \qquad (15)$$

where the spatially and angle dependent elastic functions $\{\kappa_i\}$, $i = 1, \ldots, 9$, are given in the Appendix.

By incorporating equations (6)–(8), (12) and (14), and the scaling relations given above, the following dimensionless time-dependent first-order nonlinear partial differential equation is obtained to describe surface director motion:

$$\lambda^{s*} \frac{\partial \phi}{\partial t^*} = \kappa_{10} + \kappa_{11} \frac{\partial \phi}{\partial r^*} + \kappa_{12} \frac{\partial \phi}{\partial z^*} - W \sin[2(\phi - \phi_o)] \qquad (16)$$

where the spatially and angle dependent elastic functions $\{\kappa_i\}$, $i = 10$, 11 and 12, are given in the Appendix. The new scaling relations introduced in equation (16) are for the surface viscosity ($\lambda^{s*} = 2\lambda^s/\gamma_1 R$) and surface anchoring strength ($W = 0{\cdot}5(RW_o/K)$). λ^{s*} is the ratio of the surface characteristic time τ_s to the bulk characteristic time τ_o; i.e.

$$\lambda^{s*} = \left(\frac{2\lambda^s R}{K}\right) \Big/ \left(\frac{\gamma_1 R^2}{K}\right) = \tau_s/\tau_b. \qquad (17)$$

The following three representative cases describe the effect of the surface viscosity: (*a*) $\lambda^{s*} \to 0$ corresponds to the case where surface director reorientation is caused by torques transmitted by bulk director reorientation; (*b*) $\lambda^{s*} = 1$ corresponds to comparable surface and bulk dynamics; and (*c*) $\lambda^{s*} \to \infty$ corresponds to fixed surface director orientation since $\partial\phi/\partial t^* = 0$ denotes no surface rotation. In addition, the following three representative cases describe the effect of the dimensionless surface anchoring strength: (*a*) $W \to 0$ implies that the surface dynamics are not dependent on W, but rather on λ^{s*}; (*b*) $W = 1$ implies that the surface dynamics are dependent on both W and λ^{s*}; and (*c*) $W \to \infty$ corresponds to the case of strong surface anchoring and no surface rotation being allowed. Consequently, the surface can be described as follows with respect to these cases: (*a*) the surface is viscous for $W \to 0$; (*b*) the surface is elastic for $\lambda^{s*} \to 0$; and (*c*) the surface is viscoelastic for $\lambda^{s*} = W = 1$.

The dimensionless total free energy is obtained by combining equations (5), (6), (13) and (14), and the scaling relations given above. It is expressed as follows:

$$F^* = F_d^* + F_m^* + F_s^* \qquad (18)$$

where

$$F_d^* = 2\pi \iint \left(\kappa_{13} + \kappa_{14}\frac{\partial\phi}{\partial r^*} + \kappa_{15}\frac{\partial\phi}{\partial z^*} + \kappa_{16}\frac{\partial\phi}{\partial r^*}\frac{\partial\phi}{\partial r^*} + \kappa_{17}\frac{\partial\phi}{\partial r^*}\frac{\partial\phi}{\partial z^*} + \kappa_{18}\frac{\partial\phi}{\partial z^*}\frac{\partial\phi}{\partial z^*} \right) dr^* dz^* \quad (19a)$$

$$F_m^* = -\pi Z_o \iint r^* \cos^2\phi \, dr^* dz^* \quad (19b)$$

$$F_s^* = 2\pi W \iint \sin^2(\phi - \phi_o) r^* dz^*. \quad (19c)$$

The spatially and angle dependent elastic functions $\{\kappa_i\}$, $i = 13, \ldots, 18$, are given in the Appendix. In the absence of a magnetic field, two limiting cases are obtained from the total free energy equation. In the limit of negligible surface free energy, which occurs when $W \to 0$, the equilibrium director configuration is obtained by minimizing the total distortion free energy [equation (19 *a*)]. On the other hand, in the limit of negligible distortion free energy, which happens as $W \to \infty$, the surface free energy is replaced by fixed boundary conditions.

As mentioned above there is symmetry about the z axis in bipolar droplets, and equations (15) and (16) can be solved numerically within only the half-circle where $r^* > 0$ (figure 1). Consequently, the initial and boundary conditions are as follows:

$$\phi = \phi_o(r^*, z^*) \quad \text{at} \quad t^* = 0, \quad r^* \geqslant 0, \quad -1 \leqslant z^* \leqslant 1 \quad (20a)$$

$$\frac{\partial\phi}{\partial r^*} = 0 \quad \text{at} \quad t^* \geqslant 0, \quad r^* = 0, \quad -1 \leqslant z^* \leqslant 1 \quad (20b)$$

$$\lambda^{s*}\frac{\partial\phi}{\partial t^*} = \kappa_{10} + \kappa_{11}\frac{\partial\phi}{\partial r^*} + \kappa_{12}\frac{\partial\phi}{\partial z^*} - W \sin[2(\phi - \phi_o)]$$
$$\text{at} \quad t^* \geqslant 0, \quad r^* > 0, \quad z^* = (1 - r^{*2})^{1/2}. \quad (20c)$$

The Galerkin finite element method [24], with bilinear basis functions and 200 elements, is used for the numerical solution. A set of nonlinear ordinary time-dependent differential equations are obtained after spatial discretization, which are solved simultaneously using a Newton–Raphson iteration scheme. Convergence is assumed when the length of the vector of the difference between two successive computed solution vectors is less than 10^{-6}. A finite difference method is used to discretize time and a first order implicit Euler predictor-corrector method is used for time integration. To minimize the computing time without losing accuracy, an adaptive time step control scheme [25] is used. This method takes into account the local truncation error and a user-specified tolerance; the main idea is that large (small) time steps are taken when little (significant) changes occur in the transient solution. It is noted that this method of solution is applicable to any arbitrary geometry.

Table Scaled physical constants used in present work. See text for definitions.

Constant	Values					
K_{11}^*	0·6667					
K_{33}^*	1·3333					
λ^{s*}	10^{-3}					
	10^{-3}		1		10^3	
W	1		10^{-2}		10^{-1}	
	10^1		10^2		10^3	
Z_o	10	50	100	200	300	400
	500	600	700	800	900	1000

The dependent variable is ϕ and the independent variables are (r^*, z^*, t^*). The parameters are the dimensionless splay (K_{11}^*) and bend (K_{33}^*) elastic constants, dimensionless surface viscosity (λ^{s*}), dimensionless surface anchoring strength (W), and dimensionless Zocher number (Z_o). Although a comprehensive parametric study was performed on these parameters, the restricted number of simulation results presented here (table) best reflect the objectives of this paper.

3. Results and discussion

This section presents numerical results obtained from the model outlined above, and is divided into two parts. The first part shows how the initial condition is obtained, and discusses the effects that the dimensionless surface viscosity λ^{s*} and dimensionless anchoring strength W have on director reorientation dynamics. The second part presents numerical results pertaining to magnetic-induced director reorientation dynamics in bipolar droplets. Comparison of these numerical results with experimental data found in the literature is made to validate the model presented in § 2.

3.1. *Effects of surface conditions*

Figure 2 shows the director configuration inside a bipolar droplet according to a mathematical model by Xu *et al.* [26]. This model describes reasonably well the director configuration where the liquid crystalline material properties (K_{11}^*, K_{33}^*, W) warrant a bipolar droplet. To determine the parametric envelope of K_{11}^*, K_{33}^* and W in which bipolar droplets form, the model described in § 2 was solved using the director configuration shown in figure 2 as the initial condition and with the magnetic field turned off (i.e. $Z_o = 0$). The values for K_{11}^*, K_{33}^*, λ^{s*} and W are listed in the table. The steady-state director configurations for (*a*) $W = 10^{-3}$, (*b*) $W = 1$, and (*c*) $W = 10^3$ are shown in figure 3. The

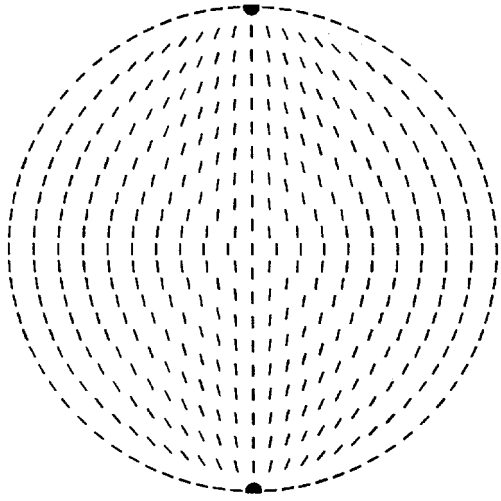

Figure 2. Calculated director configuration according to mathematical model [21]. The configuration represents reasonably well the bipolar configuration.

director configuration is bipolar at $W = 10^3$, uniform at $W = 10^{-3}$, and has an intermediate profile at $W = 1$. With respect to the discussion regarding the total free energy [equations (18) and (19)], the following two observations are made. The bipolar configuration exists only for strong surface anchoring strengths W_o, where the surface directors remain strongly anchored tangentially to the cavity wall. When the surface anchoring strength is sufficiently weak, however, the surface directors align with the bulk directors as the bulk distortion free energy is minimized. These numerical results are in agreement with Drzaic's [6] qualitative model and existing experimental data [27, 28]. It is important to note that the value of W_o [equation (6 c)] for essentially fixed anchoring is larger (smaller) for smaller (larger) droplets. This is due to the fact that as the droplet radius decreases (increases) the relative importance of bulk (surface) energy increases (decreases).

The mean magnitude of the orientation angle $\langle\|\phi\|\rangle$ defined as

$$\langle\|\phi\|\rangle = \frac{1}{\pi R^2}\int_{-1}^{1}\int_{(1-z^{*2})^{1/2}}^{(1-z^{*2})^{1/2}} \phi \, dr^* \, dz^* \qquad (21)$$

is employed in the ensuing discussion to better characterize the dynamical process. Its value at the steady state is denoted as $\langle\|\phi_{ss}\|\rangle$. Figure 4 is a semilogarithmic plot of the mean magnitude of the orientation angle at the steady state $\langle\|\phi_{ss}\|\rangle$ versus dimensionless anchoring strength W. Consistent with the director configurations shown in figure 3 and discussed above, $\langle\|\phi_{ss}\|\rangle$ increases with W in the range of $10^{-3} \leqslant W \leqslant 10^3$. This figure shows that the values chosen for W in this parametric study are appropriate since the curve is sigmoidal; i.e. $\langle\|\phi_{ss}\|\rangle$ is constant for $W \leqslant 10^{-2}$ and $W \geqslant 10^2$. Therefore, a value of $W = 10^3$ is sufficient to obtain a bipolar droplet. The value of λ^s* is not specified, because this plot gives the steady-state orientation angle, which is not affected by λ^s*. The surface viscosity does, however, affect the transient phenomena.

Since $\langle\|\phi\|\rangle$ relaxes exponentially, a relaxation characteristic time τ can be defined as the time for

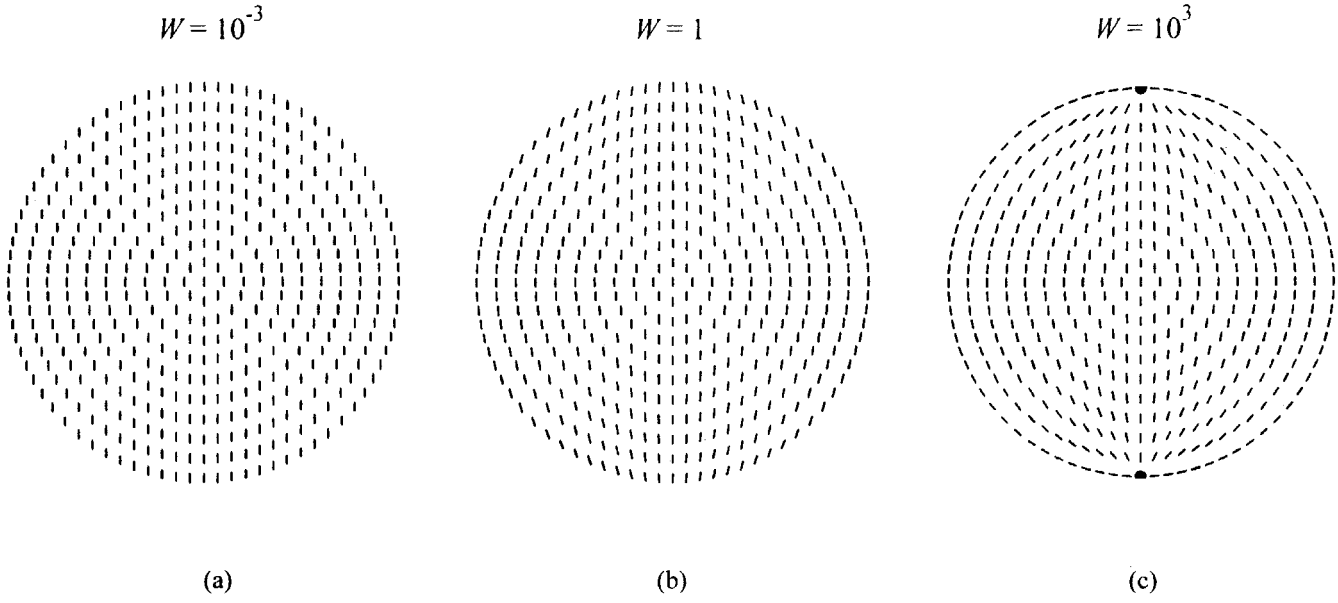

Figure 3. Steady-state director configurations for the following dimensionless surface anchoring strengths: (*a*) $W = 10^{-3}$, (*b*) $W = 1$, and (*c*) $W = 10^3$. The bipolar configuration exists in the limit of $W = 10^3$. In the limit of $W = 10^{-3}$, however, the configuration is uniform.

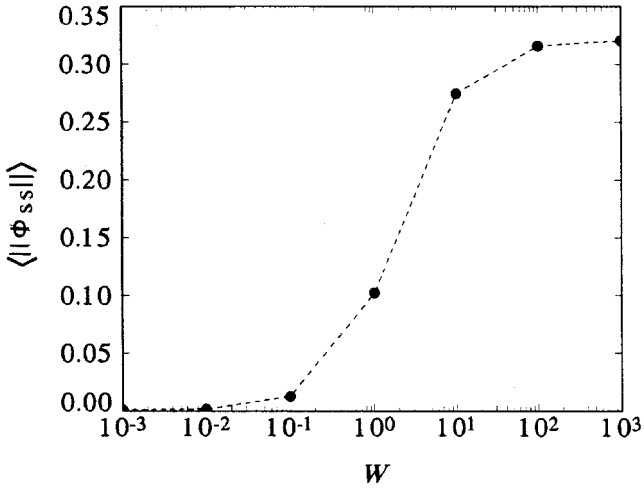

Figure 4. Mean magnitude of the orientation angle at the steady state $\langle\|\phi_{ss}\|\rangle$ versus dimensionless surface anchoring strength W. The curve is sigmoidal, indicating that the values for W in the table are appropriate for a parametric study.

$\langle\|\phi\|\rangle$ to go from $\langle\|\phi_o\|\rangle$ to $(\langle\|\phi_o\|\rangle + 0{\cdot}632\Delta_{ss})$ where $\Delta_{ss} = \langle\|\phi_{ss}\|\rangle - \langle\|\phi_o\|\rangle$. This definition for τ is similar to the definition of a time constant used in characterizing experimental data [29], where essentially a steady state is achieved at approximately four time constants. Figure 5 is a logarithmic plot of τ versus dimensionless anchoring strength W for the following dimensionless surface viscosities: $\lambda^{s*} = 10^{-3}$ (squares), $\lambda^{s*} = 1$ (triangles), and $\lambda^{s*} = 10^{3}$ (circles). For a given W in the range of $10^{-3} \leqslant W < 10^{3}$, τ increases with λ^{s*}. This is due to the

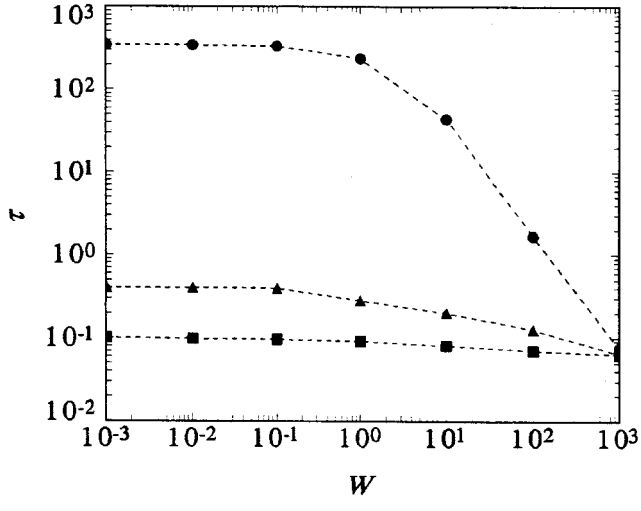

Figure 5. Characteristic time τ of the relaxation phenomena as a function of dimensionless surface anchoring strength W for the following dimensionless surface viscosities: $\lambda^{s*} = 10^{-3}$ (squares), $\lambda^{s*} = 1$ (triangles) and $\lambda^{s*} = 10^{3}$ (circles). This figure indicates that for weak anchoring τ increases with λ^{s*}. In the limit of strong anchoring, τ is independent of λ^{s*}.

fact that director reorientation dynamics is governed by both bulk and surface director reorientation. Since the surface dynamics are governed by equation (16), the rate of change of the surface director orientation decreases with increasing λ^{s*}. Consequently, it takes longer for $\langle\|\phi_o\|\rangle$ to reach $\langle\|\phi_{ss}\|\rangle$ as λ^{s*} increases. It should be noted once more that as $\lambda^{s*} \to \infty$, the strong anchoring solution is recovered. As mentioned previously, a complete discussion of the surface viscosity in magnetic-induced reorientation phenomena has been given by Rey [19].

Figure 5 also shows insights on the relationship between W and τ. In the range of $10^{-3} \leqslant W < 10^{-1}$, τ is fairly constant for any given λ^{s*}. This suggests that the surface contribution to the director reorientation dynamics is not affected by the weak surface anchoring strength, but rather by the surface viscosity. The surface is then viscous. In the range of $10^{-1} < W < 10^{3}$, however, τ decreases as W increases. This suggests that the surface contribution to the director reorientation dynamics is affected by both surface viscosity and anchoring strength, which implies the surface is viscoelastic. These phenomena are captured by the governing equation for surface director reorientation dynamics. Equation (16) shows that for low anchoring strengths ($W \ll 1$), the last term is negligible and the rate of surface director reorientation depends on λ^{s*}. Moreover, for intermediate surface anchoring strengths, ($W \cong 1$), the surface director reorientation dynamics are governed by both λ^{s*} and W. Lastly, it is apparent that τ is the same for the three λ^{s*} values at $W = 10^{3}$. This is due to the fact that the directors are strongly anchored to the surface (i.e. fixed boundary condition) and only bulk director reorientation occurs, and their dynamics are governed by bulk properties which are independent of λ^{s*}.

In summary, the bipolar droplet exists only in the case of strong anchoring ($W \geqslant 10^{3}$) and in this case the director reorientation dynamics are not affected by the surface viscosity. In the case of weak anchoring ($W < 10^{3}$), however, the director reorientation dynamics is affected by both surface viscosity and anchoring strength. In any analysis of director reorientation dynamics confined within a cavity, these two surface properties must be taken into account.

3.2. *Magnetic-induced reorientation dynamics in bipolar droplets*

Figure 6 is a plot of the mean magnitude of the orientation angle at the steady state $\langle\|\phi_{ss}\|\rangle$ versus the dimensionless Zocher number Z_o at the following dimensionless surface anchoring strengths: $W = 1$ (triangles) and $W = 10^{3}$ (circles). The initial director configurations for these simulations are the steady-state configurations obtained during the relaxation phenomena studied and

discussed in § 3.1, and are shown in figure 3. No director reorientation occurs for the case of $W = 10^{-3}$, since the initial director configuration is already uniform and parallel with the magnetic field. Consequently, the results for this case are not shown in figure 6. The curves for $W = 1$ and 10^3 decrease monotonically because the directors are being realigned along the z axis by the magnetic field. $\langle \|\phi_{ss}\| \rangle$ vanishes at high Z_o values for weak anchoring ($W = 1$), but approaches a finite value for strong anchoring ($W = 10^3$) since the surface directors cannot reorient. This means that there is a sharp transition between the bulk directors which are uniformly aligned along the z axis by the magnetic field and the surface directors which are anchored tangentially to the droplet surface. In other words, the magnetic coherence length ξ [7] is infinitely small; i.e. $\xi \to 0$. Another point to notice in figure 6 is that the absolute value of the difference $|\Delta|$ between $\langle \|\phi_{ss}\| \rangle$ at $Z_o = 0$ and $\langle \|\phi_{ss}\| \rangle$ at $Z_o = 10^3$ is greater for $W = 10^3$ ($|\Delta| = 0{\cdot}20$) than for $W = 1$ ($|\Delta| = 0{\cdot}10$). This provides insights into PDLC applications, where high contrast between the opaque 'on' state ($Z_o > 0$) and transparent 'off' state ($Z_o = 0$) is required. In general, light scattering depends on the director configuration within a droplet since the configuration affects the liquid crystal refractive indices. Wu *et al.* [1] present a simple and useful approach to relate the liquid crystal refractive indices to the bipolar configuration; although this approach is not a rigorous one, it reflects current understanding on this complex optical phenomenon. Furthermore, as will be shown below, although the results are from a single droplet and not from a sample of droplets as in a PDLC film, the numerical results and analyses are consistent with experimental data on PDLC film transmittance. Consequently, this paper provides an understanding on PDLC film operation, and is a basis for future work using more complex and rigorous models for light scattering from multiple droplets. According to Wu *et al.* [1], the average ordinary refractive index $\langle n_o \rangle$ of a bipolar droplet in the absence of an external field is greater than the ordinary refractive index n_o for a uniform director configuration that is unconfined. Hence, light is scattered since $\langle n_o \rangle > n_o = n_p$, where n_p is the polymer refractive index. As the bulk director configuration becomes more uniform from the effect of the external field, $\langle n_o \rangle$ approaches $n_o = n_p$, which means that light is less scattered. In the limit $\langle n_o \rangle = n_o = n_p$, light is not scattered by the bipolar droplet. Since $|\Delta|$ is larger for $W = 10^3$ than for $W = 1$, it is then expected that a film containing droplets with $W = 10^3$ (i.e. bipolar droplets) provides much greater contrast than a film made up of droplets with $W = 1$. The focus of the remainder of this paper is therefore on bipolar droplets. Figure 6 also provides an explanation for the typical experimental

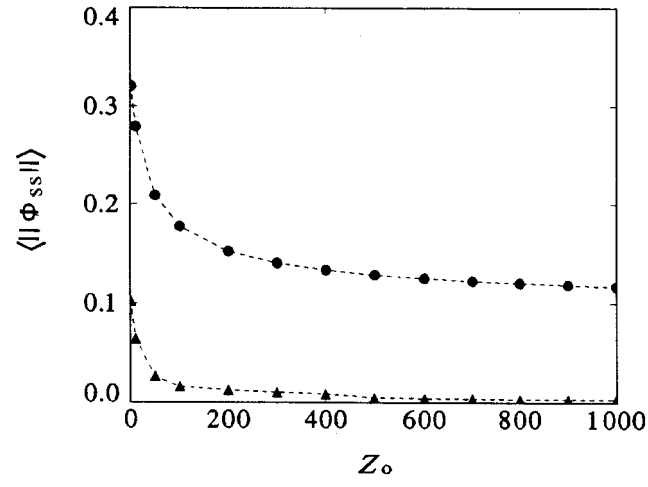

Figure 6. Mean magnitude of the orientation angle at the steady state $\langle \|\phi_{ss}\| \rangle$ versus dimensionless Zocher number Z_o at the following dimensionless surface anchoring strengths: $W = 1$ (triangles) and $W = 10^3$ (circles).

plot of light transmittance versus voltage [2, 3, 5, 6]. The light transmittance increases exponentially at low voltages, but then saturates at high voltages. This can be explained once more by noting that light scattering depends on the director configuration within the droplets. The exponential increase is due to the exponential decrease of $\langle \|\phi_{ss}\| \rangle$ as a function of the external field. Similarly, the saturation is due to the bulk directors reaching a uniform state while the surface directors remain strongly anchored tangentially to the surface. This means that director reorientation ceases and $\langle \|\phi_{ss}\| \rangle$ remains constant at the saturation value as Z_o increases.

Figure 7 is a plot of the mean magnitude of the

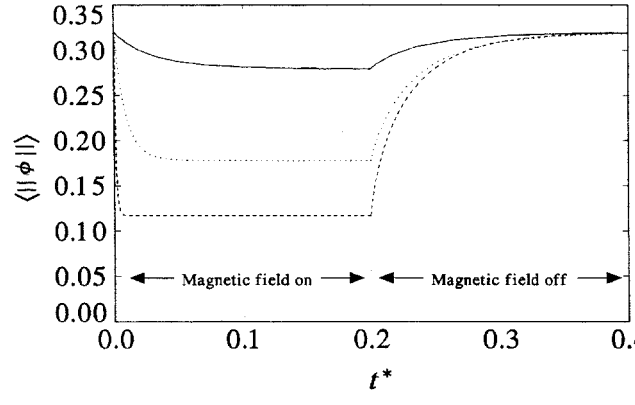

Figure 7. Mean magnitude of the orientation angle $\langle \|\phi\| \rangle$ as a function of dimensionless time t^* for the following Zocher numbers: $Z_o = 10$ (solid line), $Z_o = 10^2$ (dotted line), and $Z_o = 10^3$ (dashed line). The magnetic field is on in the time range $0 \leqslant t^* < 0{\cdot}2$, but is off in the time range $0{\cdot}2 < t^* \leqslant 0{\cdot}4$. The same curves are obtained when the magnetic field is turned on and off repeatedly.

orientation angle $\langle\|\phi\|\rangle$ versus dimensionless time t^* at the following Zocher numbers: $Z_o = 10$ (solid line), $Z_o = 10^2$ (dotted line), and $Z_o = 10^3$ (dashed line). Since these results are for bipolar droplets, $W = 10^3$. The director configurations at the steady state for these three cases are shown in figure 8. While little bulk director reorientation is observed at low fields ($Z_o = 10$), a uniform bulk orientation is obtained at higher fields ($Z_o = 10^3$). These director configurations are consistent with the multi-stage model proposed by Drzaic [13], and Jain and Rout [14] to explain their experimental data. In figure 7, the magnetic field is turned on at $t^* = 0$ and kept on during the time interval of $0 \leqslant t^* < 0{\cdot}2$, but is turned off at $t^* = 0{\cdot}2$. The same curves and director patterns in figures 7 and 8 are obtained when the magnetic field is turned on and off repeatedly. Consequently, the process is reversible. This suggests that bipolar droplets are appropriate for PDLC applications, where the field is turned on and off continuously during device operation. Consistent with the results shown in figure 6, $\langle\|\phi_{ss}\|\rangle$ decreases as Z_o increases when the magnetic field is turned on. This figure shows that when the magnetic field is turned on, $\langle\|\phi\|\rangle$ decreases exponentially and then saturates with time. Moreover, figure 7 also shows that $\langle\|\phi\|\rangle$ increases exponentially and then saturates with time after the magnetic field is turned off. This provides an explanation for the typical experimental plot of light transmittance versus time upon application and followed by removal of an external field [5]. In the on state, the light transmittance increases exponentially at early times but then saturates at late times. Once the field is turned off, however, the light transmittance decreases exponentially and then saturates with time. As explained above, light scattering

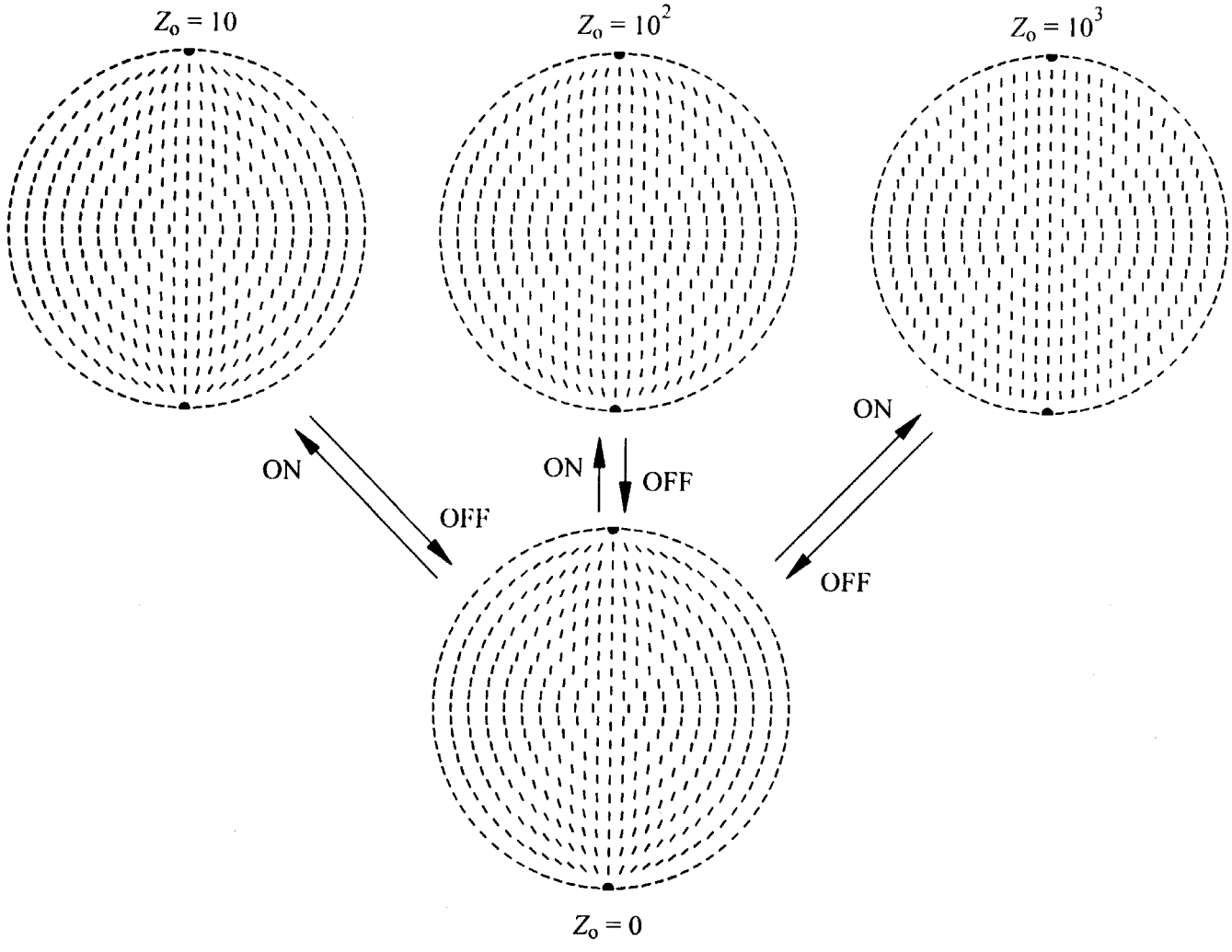

Figure 8. Steady-state director configurations corresponding to the on and off states shown in figure 7. The steady-state configuration for the off state ($Z_o = 0$) is the same for the three cases. On the other hand, the steady-state configurations are not the same in the on state where $Z_o = 10$ (top left), $Z_o = 10^2$ (top middle), and $Z_o = 10^3$ (top right). The arrows indicate that the configurations are reversible as the field is turned on and off repeatedly.

depends on the director configuration within the droplets. Therefore, the exponential increase in transmittance during the on state is due to the exponential decrease in $\langle\|\phi\|\rangle$. Moreover, the saturation at later times is due to the director configuration reaching an equilibrium state. Similarly, the exponential decrease and saturation in light transmittance in the off state is due to the exponential increase and saturation in $\langle\|\phi\|\rangle$ during the off state shown in figure 7.

In PDLC applications, the rise and decay times are employed to describe the film response. In this paper, the rise time t_r is defined as the time required for $\langle\|\phi\|\rangle$ to go from $\langle\|\phi_o\|\rangle$ to $(\langle\|\phi_o\|\rangle + 0{\cdot}9\Delta_{ss})$, where $\Delta_{ss} = \langle\|\phi_{ss}\|\rangle - \langle\|\phi_o\|\rangle$. Moreover, the decay time t_d is defined as the time required for $\langle\|\phi\|\rangle$ to go from $\langle\|\phi_{ss}\|\rangle$ to $(\langle\|\phi_o\|\rangle + 0{\cdot}1\Delta_{ss})$. These definitions are similar to the ones used in the literature to describe experimental data [30]. Figure 9 is a plot of the reciprocal dimensionless rise time versus the dimensionless Zocher number Z_o for the bipolar droplet ($W = 10^3$). The reciprocal dimensionless decay time is constant at $t_d^{*-1} \cong 12$ in the Zocher number range explored in this paper and is therefore not shown in figure 9. The reasoning behind this observation is that during the decay period $Z_o = 0$. Consequently, according to equation (15), the rate of director relaxation in this period is independent of Z_o and is just set by the bulk reorientation time τ_o [equation (17)]. These results are consistent with the following two experimental observations: (*a*) t_r^{*-1} increases linearly with the square of the field strength, and (*b*) t_d^{*-1} is independent of field strength [30]. In addition, these results are similar to the ones predicted and observed in the classical Fréedericksz transitions [23, 31]. This is due to the fact that the present geometry is a complex combination of the geometries used in studying Fréedericksz transitions.

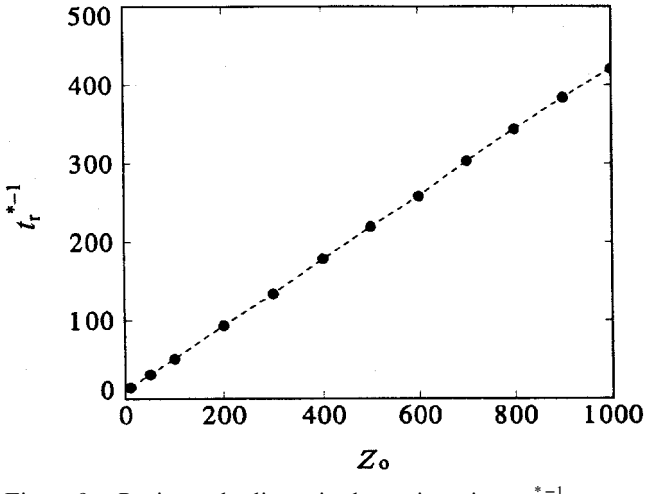

Figure 9. Reciprocal dimensionless rise time t_r^{*-1} as a function of dimensionless Zocher number Z_o. Consistent with experimental observations, the reciprocal rise time is a linear function of Z_o.

A final and important fact to notice is that the model presented in this paper is able to predict the experimental observation that the switching field strength increases linearly with the reciprocal of the droplet radius [4, 32]. In this paper, the switching field strength is defined as the field strength required for $\langle\|\phi\|\rangle$ to go from $\langle\|\phi_o\|\rangle$ to $(\langle\|\phi_o\|\rangle + 0{\cdot}9\Delta_{ss})$, which is similar to the one employed in the literature to describe experimental data [4, 32]. This relation between switching field strength and droplet radius is already contained in the definition of the dimensionless Zocher number given in § 2.2.

4. Conclusions

This paper presented numerical results from a two-dimensional study of the director reorientation dynamics inside a circle. These results are appropriate to spherical droplets where the director configuration is axisymmetric such as the bipolar droplet. The following two types of dynamics were explored: (*a*) director relaxation from a distorted configuration, and (*b*) director reorientation due to a magnetic field. The Euler–Lagrange equation was derived to govern surface director reorientation dynamics. The following three parameters were obtained in the nondimensionalization process: (*a*) the dimensionless surface anchoring strength W, (*b*) the dimensionless surface viscosity λ^s* and (*c*) the dimensionless Zocher number Z_o. The bipolar configuration exists in the strong anchoring case ($W = 10^3$), where surface directors are not permitted to rotate.

The characteristic time τ for a distorted configuration to relax to equilibrium depends on the magnitude of λ^s* and W. In the limit of strong anchoring ($W = 10^3$), τ is independent of surface properties, but is dependent on bulk properties. This means that the director reorientation dynamics in bipolar droplets are not affected by λ^s*. In the limit of very weak surface anchoring strengths ($10^{-3} \leqslant W < 10^{-1}$), τ is dependent only on λ^s*. The surface is then viscous. Lastly, τ depends on both W and λ^s* for weak but finite anchoring strengths ($10^{-1} \leqslant W < 10^3$), which implies the surface is viscoelastic. Therefore, to properly study the director reorientation dynamics confined inside cavities, both λ^s* and W must be taken into account.

The numerical solution to the model presented in this paper replicates frequently reported experimental observations on the performance of PDLCs. These observations are the following: (*a*) the light transmittance increases exponentially at first but then saturates as the external applied field increases; (*b*) the light transmittance increases exponentially initially but then saturates with time in the on state; (*c*) the light transmittance decreases

exponentially initially but then saturates with time in the off state; (*d*) the reciprocal rise time is linearly dependent on the square of the external applied field; (*e*) the reciprocal decay time is not dependent on the external applied field; and (*f*) the switching field is inversely proportional to the droplet radius. These numerical results suggest that for fast response, films containing small droplets are recommended. This requires high field strengths, but lowers the rise time and increases the film contrast between the on and off states.

This work is supported by a grant from the Natural Sciences and Engineering Research Council of Canada (NSERC).

Appendix

The elastic functions $\{\kappa_i\}$, $i = 1, \ldots, 18$, in equations (15), (16) and (19 *a*) are defined as follow:

$$\kappa_1 = -\frac{1}{2}\frac{1}{r^{*2}}K_{11}^{*}\sin(2\phi) \qquad \text{(A-1 } a\text{)}$$

$$\kappa_2 = \frac{1}{r^{*}}(K_{11}^{*}\cos^2\phi + K_{33}^{*}\sin^2\phi) \qquad \text{(A-1 } b\text{)}$$

$$\kappa_3 = \frac{1}{2}(K_{33}^{*} - K_{11}^{*})\sin(2\phi) \qquad \text{(A-1 } c\text{)}$$

$$\kappa_4 = K_{11}^{*}\cos^2\phi + K_{33}^{*}\sin^2\phi \qquad \text{(A-1 } d\text{)}$$

$$\kappa_5 = \frac{1}{2}\frac{1}{r^{*}}(K_{33}^{*} - K_{11}^{*})\sin(2\phi) \qquad \text{(A-1 } e\text{)}$$

$$\kappa_6 = \frac{1}{2}(K_{11}^{*} - K_{33}^{*})\sin(2\phi) \qquad \text{(A-1 } f\text{)}$$

$$\kappa_7 = K_{11}^{*}\sin^2\phi + K_{33}^{*}\cos^2\phi \qquad \text{(A-1 } g\text{)}$$

$$\kappa_8 = (K_{33}^{*} - K_{11}^{*})\cos(2\phi) \qquad \text{(A-1 } h\text{)}$$

$$\kappa_9 = (K_{33}^{*} - K_{11}^{*})\sin(2\phi) \qquad \text{(A-1 } i\text{)}$$

$$\kappa_{10} = -\frac{1}{2}K_{11}^{*}\sin(2\phi) + \frac{z^{*}}{r^{*}}K_{11}^{*}\sin^2\phi \qquad \text{(A-1 } j\text{)}$$

$$\kappa_{11} = -\left(r^{*}(K_{11}^{*}\cos^2\phi + K_{33}^{*}\sin^2\phi) + \frac{1}{2}z^{*}(K_{33}^{*} - K_{11}^{*})\sin(2\phi)\right) \qquad \text{(A-1 } k\text{)}$$

$$\kappa_{12} = -\left(z^{*}(K_{11}^{*}\sin^2\phi + K_{33}^{*}\cos^2\phi) + \frac{1}{2}r^{*}(K_{33}^{*} - K_{11}^{*})\sin(2\phi)\right) \qquad \text{(A-1 } l\text{)}$$

$$\kappa_{13} = \frac{1}{2}\frac{1}{r^{*}}K_{11}^{*}\sin^2\phi \qquad \text{(A-1 } m\text{)}$$

$$\kappa_{14} = \frac{1}{2}K_{11}^{*}\sin(2\phi) \qquad \text{(A-1 } n\text{)}$$

$$\kappa_{15} = -K_{11}^{*}\sin^2\phi \qquad \text{(A-1 } o\text{)}$$

$$\kappa_{16} = \frac{1}{2}r^{*}(K_{11}^{*}\cos^2\phi + K_{33}^{*}\sin^2\phi) \qquad \text{(A-1 } p\text{)}$$

$$\kappa_{17} = \frac{1}{2}r^{*}(K_{33}^{*} - K_{11}^{*})\sin(2\phi) \qquad \text{(A-1 } q\text{)}$$

$$\kappa_{18} = \frac{1}{2}r^{*}(K_{11}^{*}\sin^2\phi + K_{33}^{*}\cos^2\phi) \qquad \text{(A-1 } r\text{)}$$

References

[1] Wu, B.-G., West, J. L., and Doane, J. W., 1987, *J. appl. Phys.*, **62,** 3925.

[2] Doane, J. W., 1990, *Liquid Crystals: Applications and Uses*, edited by B. Bahadur (Singapore: World Scientific), Vol. 1, Chap. 14.

[3] Li, Z., Kelly, J. R., Palffy-Muhoray, P., and Rosenblatt, C., 1992, *Appl. Phys. Lett.*, **60,** 3132.

[4] Erdmann, J. H., Lackner, A. M., Sherman, E., and Margerum, J. D., 1993, *J. SID*, **1,** 57.

[5] Montgomery, G. P., Smith, G. W., and Vaz, N. A., 1994, *Liquid Crystalline and Mesomorphic Polymers*, edited by V. P. Shibaev and L. Lam (New York: Springer), Chap. 5.

[6] Drzaic, P. S., 1995, *Liquid Crystal Dispersions* (World Scientific).

[7] de Gennes, P. G., and Prost, J., 1993, *The Physics of Liquid Crystals*, 2nd edition (Clarendon Press).

[8] Dubois-Violette, E., and Parodi, O., 1969, *J. Phys. (Paris) Colloq.*, **30,** C4-57.

[9] Candau, S., Le Roy, P., and Debeauvais, F., 1973, *Mol. Cryst. liq. Cryst.*, **23,** 283.

[10] Vilfan, I., Vilfan, M., and Zumer, S., 1989, *Phys. Rev. A*, **40,** 4724.

[11] Huang, W., and Tuthill, G. F., 1994, *Phys. Rev. E*, **49,** 570.

[12] Ding, J., Zhang, H., Lu, J., and Yang, Y., 1995, *Jpn. J. Appl. Phys.*, **34,** 1928.

[13] Drzaic, P. S., 1988, *Liq. Cryst.*, **3,** 1543.

[14] Jain, S. C., and Rout, D. K., 1991, *J. appl. Phys.*, **70,** 6988.

[15] Wu, B.-G., Erdmann, J. H., and Doane, J. W., 1989, *Liq. Cryst.*, **5,** 1453.

[16] Crawford, G. P., Allender, D. W., Doane, J. W., 1992, *Phys. Rev. A*, **45,** 8693.

[17] Kralj, S., Zumer, S., 1995, *Phys. Rev. E*, **51,** 366.

[18] Goossens, W. J. A., 1995, *Mol. Cryst. liq. Cryst.*, **124,** 305.

[19] Rey, A. D., 1991, *Macromolecules*, **24,** 4450.

[20] Vertogen, G., and de Jeu, W. H., 1988, *Thermotropic Liquid Crystals, Fundamentals* (New York: Springer), Chap. 8.

[21] Rapini, A., and Papoular, M. J., 1969, *J. Phys. (Paris) Colloq.*, **30,** C4-54.

[22] Oliveira, E. A., Figueiredo Neto, A. M., and Durand, G., 1991, *Phys. Rev. A*, **44,** R825.

[23] Blinov, L. M., and Chigrinov, V. G., 1994, *Electrooptic Effects in Liquid Crystalline Materials* (Springer), Chap. 4.
[24] Fletcher, C. A. J., 1984, *Computational Galerkin Methods* (Springer).
[25] Finlayson, B. A., 1980, *Nonlinear Analysis in Chemical Engineering* (McGraw-Hill).
[26] Xu, F., Kitzerow, H. S., and Crooker, P. P., *Phys. Rev. E*, **49,** 3061.
[27] Drzaic, P. S., 1996, *Polymer Preprints*, **37,** 198.
[28] Amundson, K., and Srinivasarao, M., 1996, *Polymer Preprints*, **37,** 193.
[29] Holman, J. P., 1994, *Experimental Methods for Engineers*, 6th edition (New York: McGraw-Hill), Chap. 2.
[30] Mucha, M., 1991, *J. appl. Polym. Sci.*, **43,** 175.
[31] Chandrasekhar, S., 1977, *Liquid Crystals*, 1st edition (Cambridge University Press), Chap. 3.
[32] Drzaic, P. S., 1986, *J. appl. Phys.*, **60,** 2142.